Arch Environ Contam Toxicol (2015) 68:510–520
DOI 10.1007/s00244-014-0092-9

Effects of Superparamagnetic Iron Oxide Nanoparticles on Photosynthesis and Growth of the Aquatic Plant *Lemna gibba*

Lotfi Barhoumi · Abdallah Oukarroum · Lotfi Ben Taher · Leila Samia Smiri · Hafedh Abdelmelek · David Dewez

Received: 22 February 2014 / Accepted: 13 October 2014 / Published online: 13 November 2014

Abstract Toxicity of superparamagnetic iron oxide nanoparticles (SPION) was investigated in *Lemna gibba* plants exposed for 7 days to Fe_3O_4 (SPION-1), $Co_{0.2}Zn_{0.8}Fe_2O_4$ (SPION-2), or $Co_{0.5}Zn_{0.5}Fe_2O_4$ (SPION-3) at 0, 12.5, 25, 50, 100, 200 or 400 μg mL^{-1}. At < 400 μg mL^{-1} of SPION exposure, toxicity was indicated by decrease of chlorophyll content, deterioration of photosystem II (PSII) functions, strong production of reactive oxygen species (ROS), and inhibition of growth rate based on fresh weight (52–59 %) or frond number (32–49 %). The performance index of PSII activity was the most sensitive biomarker of PSII functions and decreased by 83, 86, and 79 % for SPION-1, SPION-2, and SPION-3, respectively. According to the change of these biomarkers, the exposure of SPION suspensions to *L. gibba* caused several alterations to the entire plant cellular system, which may come from both the uptake of nanoparticles and metal ions in the soluble fraction. Our results, based on the change of several biomarkers, showed that these SPION have a complex toxic mode of action on the entire plant system and therefore affects its viability. Therefore, the plant model *L. gibba* was shown to be a sensitive bioindicator of SPION cellular toxicity and thus can be used in the development of a laboratory bioassay toxicity testing.

L. Barhoumi · A. Oukarroum · D. Dewez (✉)
Département de Chimie, Université du Québec à Montréal, MontréalSucc. Centre-Ville, C.P. 8888, QC H3C 3P8, Canada
e-mail: dewez.david@uqam.ca

L. Barhoumi · H. Abdelmelek
Laboratoire de Physiologie Intégrée, Faculté des Sciences de Bizerte, Université de Carthage, 7021 Jarzouna, Tunisia

L. B. Taher · L. S. Smiri
Unité de Recherche Synthèse et Structure de Nanomatériaux UR11ES30, Faculté des Sciences de Bizerte, Université de Carthage, 7021 Jarzouna, Tunisia

Superparamagnetic iron oxide nanoparticles (SPION) are widely used for biomedical application in cancer therapy due to their unique physicochemical nanoscale properties, such as enhanced reactivity, heat, and magnetic-field generation (see review Singh et al. 2010). Although the accumulation of SPION in the environment come from natural sources, such as fire and volcanic eruptions, the extensive use of engineered SPION may contaminate the aquatic environment and interact with biotic components of the ecosystem. Indeed, engineered metallic nanoparticles (NPs) are known to be potentially cytotoxic for many aquatic organisms because they alter many cellular processes and generate reactive oxygen species (ROS) (Klaine et al. 2008; Bhatt & Tripathi 2011; Peralta-Videa et al. 2011). Therefore, the accumulation of hazardous NPs, such as SPION, in aquatic ecosystems may represent a biological risk of toxicity, which must be evaluated. However, many factors must be considered in a toxicological risk assessment such as bioavailability of NPs in aqueous solution, uptake by aquatic organisms, and potential toxicity at a cellular level. Previous toxicological studies have identified that metallic NPs possess many physicochemical characteristics—such as their size, shape, chemical composition, aggregation degree, and their solubility, which causes the release of toxic metal ions—that are directly related to their toxicity potential (Griffitt et al. 2008; Jiang et al. 2009).

In aquatic ecosystems, photosynthetic organisms represent the main source of biomass production essential for the viability of animals of higher ecological trophic levels. Furthermore, the bioaccumulation of metallic contaminants

in aquatic plants and algae can reach animal organisms, thus altering both biodiversity and the food chain of the ecosystem (Flinders 2006). However, the bioaccumulation effect of SPION causing toxic action on the plant cellular system has not been extensively examined, and the few studies on the toxicity of Fe_3O_4 NPs that were performed focused on terrestrial plant species grown hydroponically. For instance, Mushtaq (2011) reported inhibitory effects of Fe_3O_4 NPs after 6 days on cucumber (*Cucumis sativus*) seed germination and root elongation. They showed that the germination index, considering both relative root elongation and seed germination, decreased when cucumber seeds were exposed to 500, 2,500, and 5,000 μg mL^{-1} of Fe_3O_4 NPs. In another study, the effect of magnetite NP uptake and accumulation in pumpkin (*Cucurbita maxima*) plants grown hydroponically was investigated (Zhu et al. 2008). In this work, the investigators showed that at different aggregations of Fe_3O_4, NPs were taken up and translocated throughout various plant tissues (root, stem, and leaves), thus indicating NP transport pathways and bioaccumulation into the plant system. Recently, it was also shown that Fe_3O_4 NPs cause a decrease in net photosynthetic rate (based on absorbed carbon dioxide for fixation) and Chl *a* content when alga *Chlorella vulgaris* was exposed for 72 h to 100 and 200 10^3 μg L^{-1} of Fe_3O_4 NPs (Chen et al. 2012). Therefore, more studies must be performed to better understand the bioaccumulation effect of SPION on major physiological processes, such as photosynthesis and growth, of aquatic plants and algae.

Indeed, the entire physiological status of plant cells is highly dependent on photosynthetic activity, which it responsible for the supply of adenosine triphosphate and nicotinamide adenine dinucleotide phosphate involved in cellular metabolism. Therefore, any inhibition of photosynthetic processes may result in the alteration of the whole physiology of the plant cell (Seaton & Walker 1990; Gerst et al. 1994). For practical application, photosynthetic electron transport and carbon assimilation as the main indication of energy storage can be evaluated by PSII-dependent chlorophyll (Chl) fluorescence emission (Baker 2008). Particularly, the change in rapid Chl *a* fluorescence induction has been shown to be dependent on water-splitting system functions at the PSII RC and to electron transport activity related to oxido-reduction states of respective electron acceptors quinone A (Q_A), quinone B (Q_B), and plastoquinone pool (Strasser and Strasser 1995; Dewez et al. 2007). Ecotoxicological studies have shown that many photosynthetic-based fluorescence parameters can be sensitive biomarkers to both metallic and organic pollutants because these have different mechanisms of toxicity (Popovic et al. 2003; Ralph et al. 2007).

The freshwater plant *Lemna gibba* is a convenient model organism used in toxicological investigations due to its rapid reproduction rate (1–4 days), small size, and floating leaves, which permit rapid uptake of soluble compounds (Lewis 1995). Duckweeds (*Lemna* sp.) are frequently used for testing the effects of different substances on growth inhibition over a period of 7 days (OECD 2006). In this study, *L. gibba* plants were exposed to NP suspensions of Fe_3O_4 (SPION-1), $Co_{0.2}Zn_{0.8}Fe_2O_4$ (SPION-2), or $Co_{0.5}Zn_{0.5}Fe_2O_4$ (SPION-3) for 7 days to characterize their toxicity on the entire plant system by evaluating both photosynthetic processes and growth rate. These forms of SPION were selected to determine if their physicochemical properties can induce different degrees of toxicity in this plant model. Therefore, we were able to detect and characterize the toxic effects of these SPION by monitoring changes in different cellular and biochemical biomarkers.

Materials and Methods

Biological Material

The aquatic macrophyte *L. gibba* (CPCC no. 310) was obtained from the Canadian Phycological Culture Centre (Waterloo, Ontario, Canada). Plants were grown in an inorganic culture medium (pH 6.5) prepared as described in Frankart et al. (2002): KNO_3 202 μg mL^{-1}, KH_2PO_4 50.3 μg mL^{-1}, K_2HPO_4 27.8 μg mL^{-1}, K_2SO_4 17.4 μg mL^{-1}, $MgSO_4{\cdot}7H_2O$ 49.6 μg mL^{-1}, $CaCl_2$ 11.1 μg mL^{-1}, $FeSO_4{\cdot}7H_2O$ 6 μg mL^{-1}, H_3BO_3 5.72 μg mL^{-1}, $MnCl_2{\cdot}4H_2O$ 2.82 μg mL^{-1}, $ZnSO_4$ 0.6 μg mL^{-1}, $(NH_4)Mo_7O_{24}$ 0.043 μg mL^{-1}, $CuCl_2{\cdot}2H_2O$ 0.078 μg mL^{-1}, and $CoCl_2{\cdot}6H_2O$ 0.054 μg mL^{-1}. Cultures were maintained in a growing chamber (Conviron Controlled Environments, Winnipeg, Manitoba, Canada) under an illumination of 100 μE m^{-2} s^{-1} provided by cool white fluorescent lamps (Sylvania GRO-LUX F40/GS/WS, Drummondville, Canada) with a light-to-dark cycle of 16:8 h and a constant temperature of 24± 1 °C.

Synthesis of NPs

SPION as Fe_3O_4 (SPION-1), $Co_{0.2}Zn_{0.8}Fe_2O_4$ (SPION-2), and $Co_{0.5}Zn_{0.5}Fe_2O_4$ (SPION-3) were produced by the polyol method (Basti et al. 2010; Ben Tahar et al. 2012). The precursor salts $Co(CH_3CO_2)_2{\cdot}4H_2O$ (Acros, 97 %), $Zn(CH_3CO_2)_2{\cdot}2H_2O$ (Fluka, > 99 %), and $Fe(CH_3CO_2)_2$ (Acros, 95 %) were accurately weighed in the appropriate stoichiometric ratios and then dissolved in 125 mL of diethyleneglycol to reach a nominal Fe^{3+} concentration of 0.2 M. The hydrolysis ratio, h, as defined by the water to metal molar ratio, was adjusted to ≈ 1 for SPION-1 and to ≈ 10 for the two others SPION by adding a small amount of distilled water. The resulting mixture was then

heated to reflux under mechanical stirring for 3 h. After slow cooling, the resulting precipitate was washed with ethanol under sonication with intermittent centrifugation and dried in air at 60 °C.

Physicochemical Characterization

Powders were characterized by X-ray diffraction (XRD) on a PANalytical X'pert Pro in the 2Θ (°) range 10–90 with a scan step of 0.05 using the CoK_{α} radiation ($\lambda = 0.1789/0.1792$ nm). The unit cell parameter and peak indexing were performed with the program McMaille (Le Bail 2004), and the refinement was performed by the least squares method. The average crystal size was inferred from the broadening of the (311) diffraction line (2θ (°) $\approx$ 41) by applying the well-known Scherrer equation and considering a pseudo–Voigt line profile shape with a polycrystalline silicon as standard.

The size and shape of the prepared particles were analyzed on a JEOL-100-CX II transmission electron microscope (TEM) operating at 100 kV equipped with an energy-dispersive spectrometer with a probe diameter of 200 nm, which also provides the different metallic atomic ratios. The powders were ultrasonically dispersed in a solution of oleic acid in heptane (5 % weight). One drop of the suspension was deposited on a carbon-coated copper grid, and the solvent was evaporated at room temperature. TEM image treatment (mean particle size and shape) was made from at least 250 particles collected from 10 micrographs using the software package SAISAM (Microvision Instruments S.A.S., Evry cedex, France).

In the preparation of stock solutions, SPION were suspended in culture medium and homogenized by vortexing for 1 min, and then the solution was sonicated in ultrasonication bath for 30 min at 4 °C to break up aggregates. After sonication, particles in suspension were vortexed (1 min), and all of the concentrations of SPION used for treatment were prepared in culture medium of *L. gibba*. Furthermore, the zeta potential of SPION in culture medium was determined by the electrophoretic mobility method using a ZetaPlus particle sizer (Brookhaven Instrument, USA) with 90Plus Particles Sizing software (Ver. 4.20).

Experimental Treatments

Three triple-fronded plants were used for experiments and were placed in Petri dishes (with open lid) containing 6 mL of growth medium and initial concentrations of 0, 12.5, 25, 50, 100, 200, or 400 μg mL^{-1} of SPION. Plants were monitored for 7 days. For each experiment, all treated and control media were renewed every 24 h to maintain constantly the exposure of *L. gibba* plants to initial concentration of SPION and their soluble fraction.

Growth-Inhibition Test

Plant growth was determined by the change in fresh weight or frond number every day for 7 days. The relative growth rate (RGR) was evaluated according to Hoffmann and Poorter (2002) as RGR = (ln W_{d7}− ln W_{d0})/7 days where W_{d7} represents the fresh weight or frond number of plants at day 7, and W_{d0} represents the initial fresh weight or frond number. The inhibitory response for specific growth rate in percentage (Ir) was determined by frond number or fresh weight according to Organisation for economic Co-operation and Development (OECD) guidelines for the testing of chemicals (OECD 2006) as follows: Ir = ((μC– μT)/μC) × 100 where Ir represents the inhibitory response (in %) for the average specific growth rate; μC represents the mean value of frond number or fresh weight in the control group; and μT represents the mean value in the treatment group.

Chl Content

At 7 days of treatment, entire plants were homogenized in 100 % methanol in darkness. Then total Chl was extracted at 65 °C for 10 min and centrifuged for 5 min at 10,000 *g*. The content was determined spectrophotometrically (spectrophotometer Perkin-Elmer Lambda 40) according to Wellburn (1994) as follows: total Chl (μg mL^{-1}) = (24.93 × $A_{652.4}$ + 1.44 × $A_{665.2}$).

Fe, Co, and Zn Content in Plant Biomass

After treatment, plants were dried at 105 °C for 24 h and weighed to determine dry weight. Then plants were placed in an acid-washed glass tube containing 4 mL of HNO_3 and 500 μL of H_2O_2. The digestion process was performed during 48 h at 129 °C before dilution in MilliQ purified water for atomic absorption spectrometry (Varian SpectrAA 220 FS) quantification of iron (Fe), cobalt (Co), and zinc (Zn). Obtained Fe, Co, and Zn concentrations were normalized to dry weight.

Soluble Fraction of Fe, Co, and Zn

Solubility of free Fe, Co, and Zn released from SPION suspensions were determined in *L. gibba* medium. SPION suspensions were incubated during 24 h under the same conditions as described previously for *L. gibba*. After incubation, NPs were removed by centrifugation at 12,000*g* for 30 min. The supernatant was removed with care and diluted in 10 % HNO_3. Quantification of free Fe, Co, and Zn in solution was determined by atomic absorption spectrometry (Varian SpectrAA 220 FS).

Chl Fluorescence Measurement

Photosynthetic electron transport was monitored from the change in the rapid increase of Chl *a* fluorescence emission using a Plant Efficiency Analyser fluorometer (Hansatech, King's Lynn, Norfolk, UK). Before measurements, plants were placed in darkness for 30 min. The fluorescence induction was triggered using a 6-second saturating flash at 3,500 μE m^{-2} s^{-1}. Fluorescence intensities at O (F_O), K (F_K), J (F_J), and I (F_I) transients were determined at 20, 300 μs, 2, and 30 ms, respectively. Fluorescence intensity at *P* level reaches maximal value (F_M) under saturating illumination. Different photosynthetic-based fluorescence parameters related to the functional state of PSII were calculated according to Strasser et al. (2004) as follows: The maximum quantum yield of primary photochemistry of PSII—i.e., $F_V/F_M = (F_M - F_O)/F_M$—was used to measure the maximum efficiency of PSII electron transport. The absorption of photons by light-harvesting antenna (ABS) per active reaction center (RC), estimating the relative size of PSII light-harvesting antenna complexes, was determined by the ratio $\text{ABS/RC} = ((F_K - F_O)/0.250) \times (1/(F_J - F_O)) \times (F_M/(F_M - F_O))$. The relative variable fluorescence yield at J transient was calculated according to $V_J = (F_J - F_O)\ (F_M - F_O)$, thus estimating the fraction of Q_A in its reduced state.

ROS Formation Per Viable Cells

The formation of ROS in *L. gibba* fronds was determined according to the procedure explained in Babu et al. (2003). After being washed in culture medium, plants were exposed to 5 μM of 2′,7′dichlorodihydrofluorescein diacetate in 1 mL of solution medium for 30 min at 25 °C. The formation of ROS was determined using a fluorescence plate reader (SpectraMax M2e MultiMode Microplate Reader). The fluorescence emission was measured at 530 nm by using a light excitation wavelength at 485 nm. Fluorescence data were normalized by fresh weight.

Viability of *L. gibba* plant cells was estimated using the fluorescein diacetate (FDA) method according to Mayer et al. (1997). Four intact plants from each treatment and control were exposed to 5 μM of FDA in 1 mL of solution medium. A light excitation at 485 nm was used to measure the fluorescence emission at 530 nm. Fluorescence data were normalized by fresh weight. The ratio of ROS level per cellular viability was evaluated to normalize the formation of ROS in *L. gibba* fronds.

Statistical Analysis

All treatments were performed in two exposure test series with three replicates. Means and SDs were calculated for each treatment. Significant differences between control and treated plants were determined by one way analysis of variance and Dunnett's multiple comparison test and were determined for $p < 0.05$. The half maximal effective concentration (EC_{50}) was obtained by the inhibitory concentration *versus* the response fitting to the toxicity data.

Results

Physicochemical Characteristics of SPION

XRD is a rapid analytical technique used for phase identification of a crystalline material providing information on unit cell dimensions. The XRD patterns of all prepared powders are shown in Fig. 1a. All diffraction lines are consistent with those of typical spinel-like ferrites without evidence of impurities. The calculated cell parameters (Table 1) are close to those reported for ferrites with similar chemical composition (Vaidyanathan et al. 2007). In addition, the diffraction peaks are clearly broadened as the result of decreased particle size. The estimated crystallite average size ($size_{xrd}$) is approximately 10 nm for SPION-1 and 5 nm for SPION-2 and SPION-3. TEM images of the prepared powders are also given in Fig. 1b. They consist of approximately spherical NPs, almost nonagglomerated, with an average diameter ($size_{tem}$) of 9 nm for SPION-1 and 4 nm for others NPs. We noticed that the concordance of particle size inferred from XRD and TEM indicated that the produced NPs could be considered as single crystals. Measurement of zeta potential indicated that SPION are negatively charged in the media, and values were −26.37, −26.05, and −79.15 for SPION-1, SPION-2, and SPION-3, respectively (Table 1). These values were found to be stable in the culture medium during the experimental exposure.

Solubility and Bioaccumulation of Fe, Co, and Zn

Because all treated and control media were renewed every 24 h, the soluble fraction of free Fe, Co, and Zn released from all SPION suspensions was determined in culture medium for that time period (Fig. 2). The quantity of free Fe, Co, and Zn in aqueous solution was dependent on metal species, SPION physicochemical characteristics, and concentration. According to our results, the quantity of free Fe was dependent on SPION-1 (Fe_3O_4) concentration and increased significantly ($p < 0.05$) by 2-fold for 400 μg mL^{-1} of SPION-1 suspensions compared with exposure concentration of 12.5 μg mL^{-1}. However, free Fe per total Fe was equal to 0.6 % for 400 μg mL^{-1} of SPION-1 compared with 10.6 % for an exposure concentration of 12.5 μg mL^{-1}. Such solubility was different for SPION-2 ($Co_{0.2}Zn_{0.8}Fe_2O_4$), for which the quantity of free Fe, Co, and Zn significantly

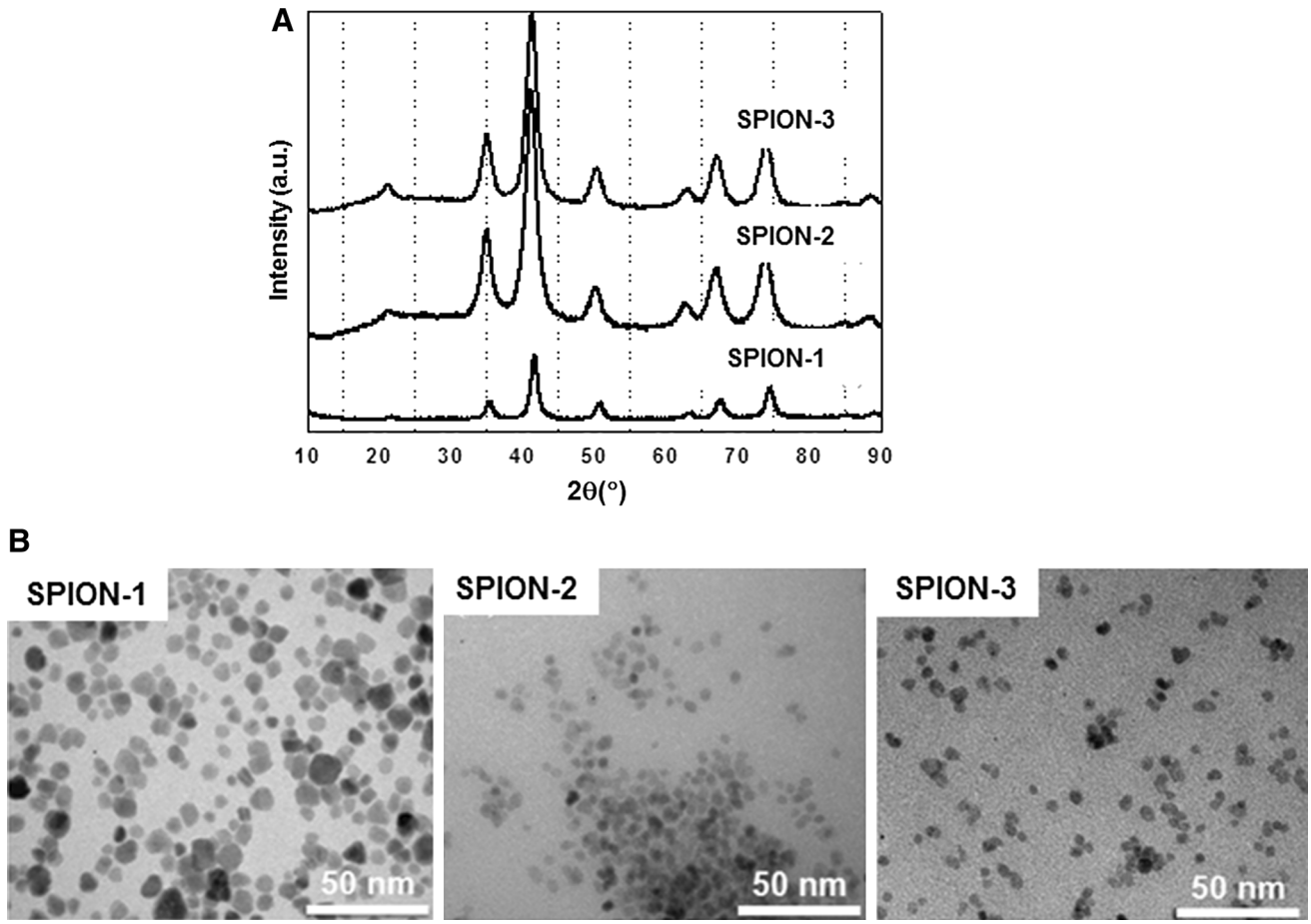

Fig. 1 XRD patterns (**a**) and TEM images (**b**) of SPION-1 (Fe_3O_4), SPION-2 ($Co_{0.2}Zn_{0.8}Fe_2O_4$), and SPION-3 ($Co_{0.5}Zn_{0.5}Fe_2O_4$)

Table 1 Microstructural characteristics of prepared SPION NPs

SPION	Cell parameter/nm	$Size_R$ (nm)	$Size_{TE}$ (nm)	Zeta potential (mV)
1	0.8390 (6)	10	9 ± 0.8	−26.37 ± 2.20
2	0.8422 (3)	5	4 ± 0.4	−26.05 ± 0.86
3	0.8433 (2)	5	4 ± 0.7	−79.15 ± 5.69

($p < 0.05$) increased respectively by 1.5-, 5.5-, and 22.5-fold at 400 μg mL^{-1} compared with 12.5 μg mL^{-1}. However, the quantity of free metals in the soluble fraction compared with exposure concentration of SPION-2 (400 μg mL^{-1}) decreased significantly ($p < 0.05$) by 13.4, 7.2, and 4 % for Fe, Co, and Zn, respectively. Furthermore, the concentration of Fe, Co, and Zn in the soluble fraction significantly ($p < 0.05$) increased, respectively, by 1.4-, 2.4-, and 1.5-fold for SPION-3 ($Co_{0.5}Zn_{0.5}Fe_2O_4$) treatment of 400 μg mL^{-1} compared with 12.5 μg mL^{-1}. However, the quantity of free Fe, Co, and Zn, compared with the treatment (400 μg mL^{-1}), decreased significantly ($p < 0.05$) by 26, 18, and 32 %, respectively. In addition, the quantity of free Zn in the soluble fraction was greater than that of Co and Fe for SPION-2 and SPION-3, respectively, and this was dependent on the composition and amount of total Zn made in the SPION (Fig. 2). Therefore, these results indicated that the concentration of Fe, Co, and Zn in the soluble fraction was dependent on the quantity of SPION suspensions in the media. Moreover, the contribution of free Fe, Co, and Zn provided by the culture medium was negligible when compared with their total amount in the soluble fraction (see Biological Material).

The bioaccumulation of total Fe, Co, and Zn was also quantified in plant biomass for *L. gibba* exposed 7 days to SPION (Fig. 3). The accumulated Fe, Co, and Zn concentrations in plants were highly dependent on the exposure concentration of SPION. The bioaccumulation of Fe increased significantly ($p < 0.05$) by almost 10-fold when *L. gibba* was exposed for 7 days to 400 μg mL^{-1} of SPION-1 compared with 12.5 μg mL^{-1}. However, the bioaccumulation of Zn was greater when *L. gibba* was exposed

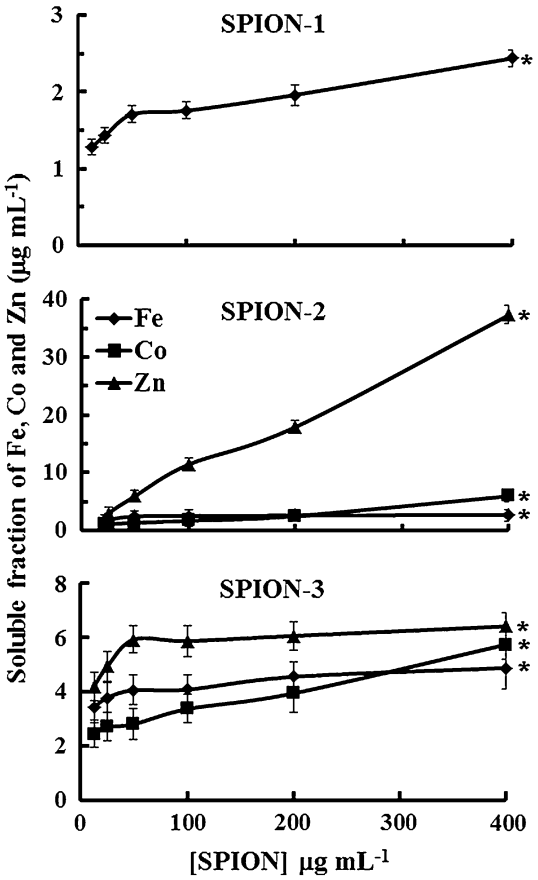

Fig. 2 Soluble fraction of Fe, Co, and Zn released from different concentrations of SPION-1 (Fe_3O_4), SPION-2 ($Co_{0.2}Zn_{0.8}Fe_2O_4$), and SPION-3 ($Co_{0.5}Zn_{0.5}Fe_2O_4$) suspensions in *L. gibba* medium after 24 h of exposure. Samples exposed to SPION were significantly different from the control at $p < 0.05$ (*)

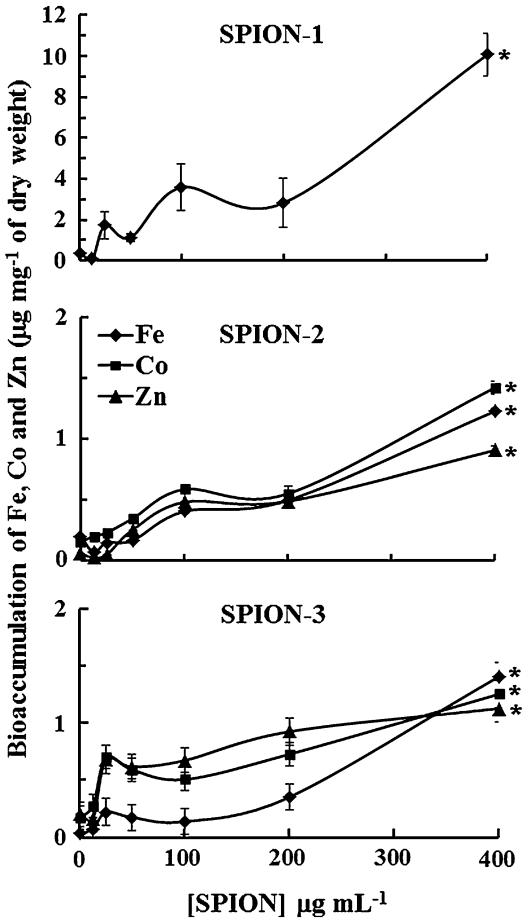

Fig. 3 Content of Fe, Co, and Zn in *L. gibba* plant exposed for 7 days to different concentrations of SPION-1 (Fe_3O_4), SPION-2 ($Co_{0.2}Zn_{0.8}Fe_2O_4$), and SPION-3 ($Co_{0.5}Zn_{0.5}Fe_2O_4$) suspensions. For SPION-1 and -3, samples exposed to 25 μg mL^{-1} were significantly different from the control at $p < 0.05$ (*). For SPION-2, samples exposed to 50 μg mL^{-1} were significantly different from the control at $p < 0.05$ (*)

to SPION-2 compared with SPION-3 under similar exposure concentrations (Fig. 3).

Inhibition of Plant Growth

When *L. gibba* plant was exposed for 7 days to SPION at concentrations varying from 12.5 to 400 μg mL^{-1}, a decrease in relative growth rate based on fronds number and fresh weight was noticed (Table 2). The relative growth rate based on fresh weight was more affected by SPION toxicity compared with frond number. Under a concentration exposure of 400 μg mL^{-1}, the relative growth rate based on fresh weight decreased significantly ($p < 0.05$) compared with the control by 37, 43.5, and 36.5 % for SPION-1, SPION-2, and SPION-3, respectively (Table 2). In addition, the inhibitory responses for specific growth rate based on fresh weight were 56, 59, and 52 % for SPION-1, SPION-2, and SPION-3, respectively (Fig. 4). However, the inhibitory responses for specific growth rate based on frond number were, respectively, 39, 51, and 49 % for SPION-1, SPION-2, and SPION-3. Moreover, when *L. gibba* plants were exposed for 7 days to different concentrations of SPION suspensions, the EC_{50} value of plant growth based on fresh weight was 244, 183, and 237 μg mL^{-1}, respectively, for SPION-1, SPION-2, and SPION-3.

Inhibition of Photosynthesis

When *L. gibba* plant was exposed 7 days to SPION concentrations varying from 12.5 to 400 μg mL^{-1}, the inhibitory effect of SPION was showed by a significant ($p < 0.05$) decrease of Chl content compared with the control by 51, 60, and 58 % for SPION-1, SPION-2, and SPION-3, respectively (Fig. 5). The Chl *a*/*b* ratio increased significantly ($p < 0.05$) compared with the control by 115, 156, and 132 %, respectively, for SPION-1, SPION-2, and

Table 2 Change in RGR based on fresh weight or frond number of *L. gibba* plants exposed for 7 days to different SPION suspensions

SPION (μg mL^{-1})	Growth parameter	RGR (μ d^{-1} or g d^{-1})		
		SPION-1	SPION-2	SPION-3
Control	FN	**0.341** ± 0.002	**0.303** ± 0.007	**0.339** ± 0.002
	FW	**0.302** ± 0.014	**0.347** ± 0.020	**0.348** ± 0.029
12.5	FN	**0.316** ± 0.005	**0.276** ± 0.007	**0.308** ± 0.008
	FW	**0.244** ± 0.030	**0.341** ± 0.024	**0.339** ± 0.02
25	FN	**0.307*** ± 0.004	**0.269*** ± 0.002	**0.307*** ± 0.004
	FW	**0.279*** ± 0.032	**0.322*** ± 0.028	**0.308*** ± 0.027
50	FN	**0.305*** ± 0.007	**0.268*** ± 0.013	**0.302*** ± 0.006
	FW	**0.276*** ± 0.038	**0.273*** ± 0.012	**0.278*** ± 0.015
100	FN	**0.298*** ± 0.004	**0.245*** ± 0.014	**0.291*** ± 0.008
	FW	**0.249*** ± 0.039	**0.265*** ± 0.006	**0.260*** ± 0.016
200	FN	**0.294*** ± 0.011	**0.231*** ± 0.032	**0.270*** ± 0.019
	FW	**0.205*** ± 0.027	**0.233*** ± 0.014	**0.238*** ± 0.004
400	FN	**0.270*** ± 0.004	**0.202*** ± 0.008	**0.237*** ± 0.052
	FW	**0.190*** ± 0.014	**0.196*** ± 0.006	**0.221*** ± 0.011

Bold data represent the mean of $n = 6$

FW fresh weight; *FN* frond number

* Significant differences for $p < 0.05$ between control and treated plants

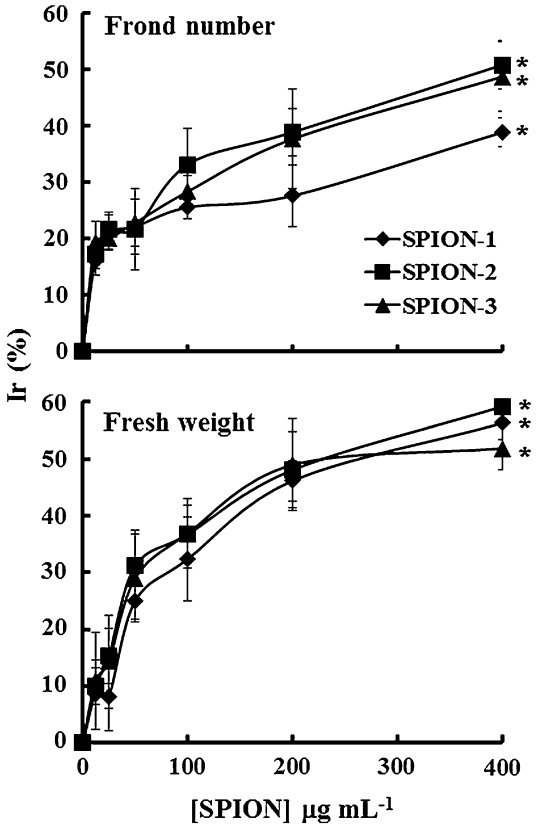

Fig. 4 Inhibitory response of *L. gibba* plant growth (% Ir of total frond number or biomass as fresh weight) after exposure for 7 days to different concentrations (12.5–400 μg mL^{-1}) of SPION-1 (Fe_3O_4), SPION-2 ($Co_{0.2}Zn_{0.8}Fe_2O_4$), and SPION-3 ($Co_{0.5}Zn_{0.5}Fe_2O_4$) suspensions. Samples exposed to SPION were significantly different from the control for $p < 0.05$ (*)

SPION-3, thus indicating a stronger inhibition of Chl *b* synthesis. The change of photosynthetic electron transport was also investigated to determine SPION toxic effects on processes related to PSII activity. The effect of SPION on primary photochemical reactions of PSII was monitored using Chl *a* fluorescence emission. We found a significant decrease of fluorescence yields at J, I, and P levels, which was related to SPION concentration without any changing in their time of appearance on the kinetics (data not shown). Furthermore, we were able to characterize in more detail the SPION effect on PSII photochemistry by using the change of photosynthetic-fluorescence parameters estimated from the fluorescence kinetic (Fig. 6). A significant effect on photosynthetic electron transport was observed at < 400 μg mL^{-1} of SPION treatment. However, there was not a significant decrease in the value of the maximal quantum yield of PSII (F_V/F_M) for SPION-1, SPION-2, and SPION-3, thus indicating that a large proportion of PSII was still able to perform primary photochemical reactions. The change of V_J values (Fig. 6) was indicative of a significant ($p < 0.05$) increase of $Q_A^-/Q_{A(total)}$ due to inhibition of PSII electron transport flow toward the plastoquinone pool. The value of ABS/RC also increased significantly ($p < 0.05$) compared with the control by 42, 70, and 39 %, respectively, for SPION-1, SPION-2, and SPION-3, thus indicating a decrease of functional PSII RCs. Moreover, the change of the PSII performance index was used as a global parameter integrating all PSII photochemical reactions. When *L. gibba* plants were exposed during 7 days to 400 μg mL^{-1}

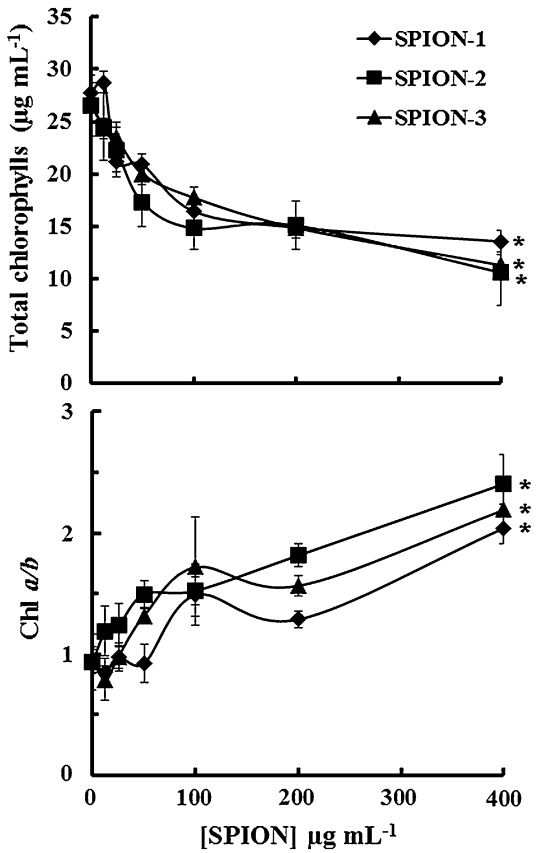

Fig. 5 Change in total Chl and ratio of Chl *a/b* when *L. gibba* plant was exposed for 7 days to different concentrations of SPION-1 (Fe_3O_4), SPION-2 ($Co_{0.2}Zn_{0.8}Fe_2O_4$), and SPION-3 ($Co_{0.5}Zn_{0.5}Fe_2O_4$) suspensions. For total Chl, samples exposed to 25 µg mL^{-1} SPION were significantly different from the control ($p < 0.05$ (*). For the ratio of Chl *a/b*, samples exposed to SPION-2 and -3 at 50 µg mL^{-1} and to SPION-1 at 100 µg mL^{-1} were significantly different from the control at $p < 0.05$ (*)

of SPION, the PI value showed a significant decrease ($p < 0.05$) compared with the control by 83, 86, and 79 % for SPION-1, SPION-2, and SPION-3, respectively (Fig. 6). Under the same experimental conditions, the EC_{50} on the change of parameter PI was 57, 17, and 200 µg mL^{-1} for SPION-1, SPION-2, and SPION-3, respectively.

Production of ROS per Viable Cells

The formation of ROS per viable cells was determined for *L. gibba* plants exposed 7 days to SPION (Fig. 7). When *L. gibba* plants were exposed 7 days to 200 and 400 µg mL^{-1} of SPION, the production of ROS increased significantly ($p < 0.05$) compared with control, thus indicating induce cellular oxidative stress under these conditions. Moreover, in *L. gibba* plants exposed for 7 days to 400 µg mL^{-1} of SPION, the production of ROS per viable cells increased by 2-fold for SPION-1 and SPION-2 compared with SPION-3.

Discussion

Alteration of Plant Physiological Status

This study showed original results concerning the toxic effects of SPION on *L. gibba* fronds, suggesting a complex mode of action that was dependent on SPION chemical composition, concentration, and dissolved metallic ions. On one hand, the bioaccumulation of free Fe, Co, and Zn from the soluble fraction contributes to the toxicity in the plant system. Solubilisation of metallic NPs into free metal ions is usually considered one of the most common mechanisms causing toxic effects in aquatic organisms (Franklin et al. 2007; Aruoja et al. 2009). However, the soluble fraction per total SPION was not proportional when comparing low (12.5 µg mL^{-1}) with high (400 µg mL^{-1}) initial concentrations of SPION. Indeed, the ratio of the concentration of free Fe, Co, and Zn contents per total concentration of SPION decreased with increasing concentration of SPION, thus indicating a change in their physicochemical properties related to their solubility. In contrast, the bioaccumulation of Fe, Co, and Zn, as well as their effects in *L. gibba* plant, increased with the increasing exposure concentration of SPION, suggesting that SPION suspensions also contribute to the toxicity impact. Recently, it was shown for agglomerates of Fe_3O_4 that NPs accumulate into the entire plant system and thus represent a source of toxicity (Zhu et al. 2008; Mushtaq 2011). Moreover, the ROS level per cell viability was greatest at an exposure SPION concentration of 400 µg mL^{-1} when the bioaccumulation of Fe, Co, Zn reached the greatest levels. Previous studies showed that many metallic NPs induce production of ROS by way of Fenton reaction or the disruption of physiological processes (Klaine et al. 2008; Hu et al. 2009). Therefore, the toxicity caused by bioaccumulated Fe, Co, and Zn in plant biomass may be due to both free ionic metals released from SPION in the soluble fraction as well as bioaccumulated SPION. However, no current analytical approach permits discrimination of the toxicity contribution between SPION and its free ionic metals.

Significance of Photosynthetic-Based Fluorescence Parameters

It was reported earlier that metals such as cadmium, copper, and chromium ions directly inhibit PSII electron transport at the water-splitting system of the RC (Küpper et al. 2002; Popovic et al. 2003; Dewez et al. 2005; Ait Ali et al. 2006). Here we showed evidence that changes of selected photosynthetic-based fluorescence parameters were indicative of the alteration of PSII functional integrity caused by SPION effects, especially under high exposure concentration

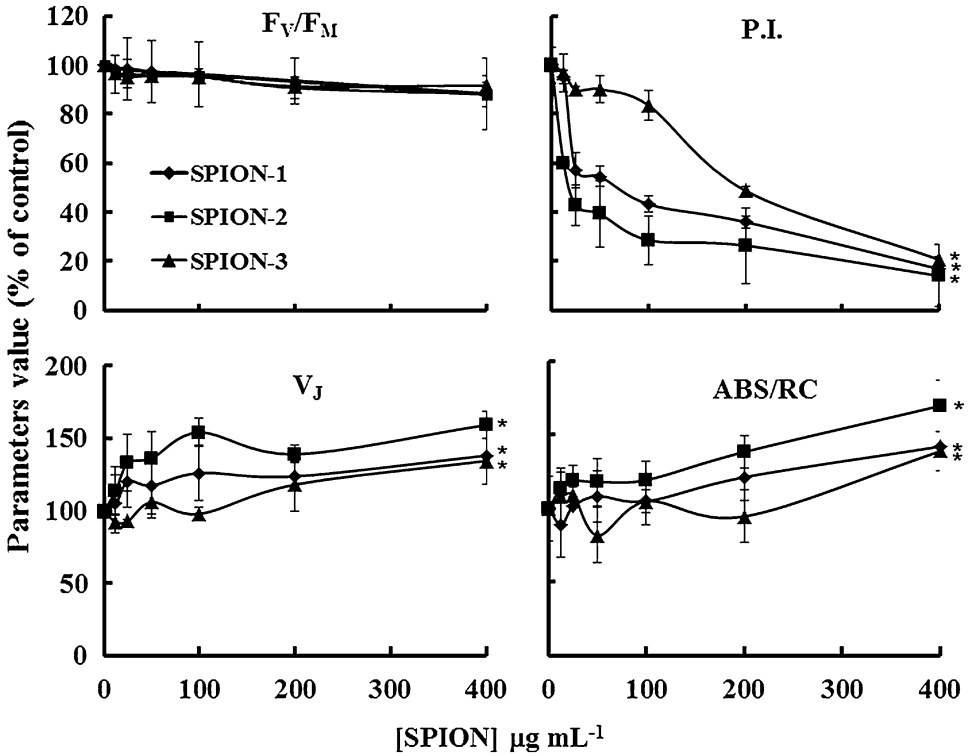

Fig. 6 Change of different photosynthetic-based fluorescence parameters when *L. gibba* plant was exposed for 7 days to different concentrations of SPION-1 (Fe_3O_4), SPION-2 ($Co_{0.2}Zn_{0.8}Fe_2O_4$), and SPION-3 ($Co_{0.5}Zn_{0.5}Fe_2O_4$) suspensions. F_V/F_M = maximal PSII quantum yield; ABS/RC = ratio between the number of active PSII RCs and light-harvesting Chl antenna size; relative variable fluorescence yield at J transient V_J; PI = performance index of PSII photochemical activity. For ABS/RC and V_J, samples exposed to 400 µg mL^{-1} of SPION were significantly different from the control for $p < 0.05$ (*). For PI, samples exposed to SPION-1 and -3 from 25 µg mL^{-1} and to SPION-2 from 12.5 µg mL^{-1} were significantly different from the control at $p < 0.05$ (*)

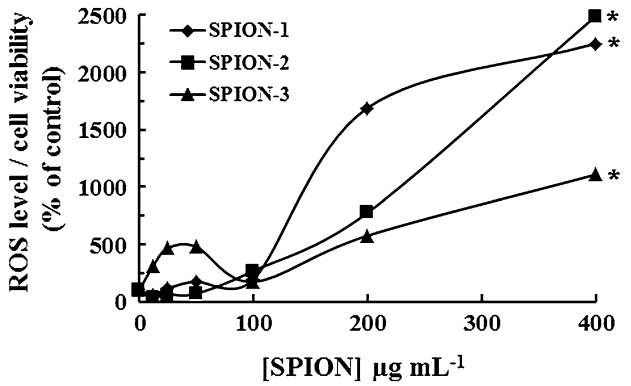

Fig. 7 Change in the production of ROS per viable cells when *L. gibba* plant was exposed for 7 days to different concentrations of SPION-1 (Fe_3O_4), SPION-2 ($Co_{0.2}Zn_{0.8}Fe_2O_4$), and SPION-3 ($Co_{0.5}Zn_{0.5}Fe_2O_4$) suspensions. Samples exposed to 100 µg mL^{-1} of SPION increased significantly in ROS compared with the control at $p < 0.05$ (*)

(400 µg mL^{-1}). By using the yields of fluorescence transients, we were able to evaluate the performance index of PSII activity, which represents an integrative indicator of all PSII photochemical reactions (Strasser et al. 2004). Compared with others fluorescence parameters, change in PI value was the most sensitive biomarker of the deteriorated PSII functions caused by all SPION toxicity. In a previous study, change of PI value was indicative of the decreased number of active PSII RCs as well as damage to the oxygen-evolving complex when *Spirodela polyrhiza* was exposed to chromate toxic effects (Appenroth et al. 2001). In our study, a high concentration of SPION (400 µg mL^{-1}) showed evidence of strong inhibitory effects on energy transfer, from light-harvesting complex to photosynthetic RCs, on the deterioration of the PSII water-splitting system and the inactivation of PSII RCs.

Comparison Between SPION-1, SPION-2, and SPION-3

Currently, there are almost no data available concerning the toxicity of SPION on aquatic organisms. Only one study concerned the toxic effects of Fe_3O_4 NPs (35 nm) on the green alga *Chlorella vulgaris* exposed during 72 h and showed induction of oxidative stress and alteration of photosynthesis under treatment from 200 to 1,600 µg mL^{-1} (Chen et al. 2012). In our study, according to the change of

used cellular and biochemical biomarkers, the exposure of SPION-1, SPION-2, and SPION-3 suspensions to *L. gibba* caused several alterations to the entire plant cellular system. However, based on our results, we were not able to compare the complex toxicity mechanisms between SPION-1, SPION-2, and SPION-3 suspensions, which may come from both the uptake of NPs and the presence of metal ions in the soluble fraction. Indeed, no current protocols and analytical methods permit the precise quantification of the proportion of bioaccumulated NPs from metal ions in plant cells without altering their physicochemical states or the determination of their contributions to the impact of cellular toxicity. Therefore, this study permitted only the detection and characterization of the toxic effects of these SPION by monitoring changes in different cellular and biochemical biomarkers.

Ecotoxicological Significance

The toxic potential of SPION suspension as hazardous contaminants in the aquatic environment must be investigated to develop specific bioassays for toxicity assessment. Our results showed that the toxicity risk of SPION suspension in aqueous solution can be estimated by the physiological alteration of the aquatic plant *L. gibba*. In this regard, the *L. gibba* plant was shown to be a sensitive bioindicator of SPION toxicity in laboratory bioassay testing. However, in a natural freshwater environment, more factors may alter the physicochemical properties of NPs in aqueous solution, which must be investigated. Indeed, the agglomeration and sedimentation of SPION can be affected by natural organic colloids, which may modify their bioavailability by changing their solubility. It has been shown that the presence of humic and fulvic acids in the natural environment may cause sedimentation of several NPs (Domingos et al. 2009; Scown et al. 2010). Therefore, further studies should be aimed at determining the behaviour of SPION in the aquatic environment and how natural conditions can alter their potential source of toxicity.

Conclusion

In this study, we characterized the toxicity of three SPION suspensions having different chemical compositions on the aquatic plant model *L. gibba*, which was shown to be a valuable bioindicator of toxicity. The toxicity impact was indicated by physiological alterations such as decreased Chl content, deterioration of photosynthetic activity, induction of oxidative stress, and inhibition of growth. Our results, based on the change of several biomarkers, showed that these SPION have a complex toxic mode of action on the plant system, thus affecting its viability. Therefore, the plant model *L. gibba* was shown to be a sensitive bioindicator of SPION cellular toxicity and thus can be used in the development of laboratory bioassay toxicity testing.

Acknowledgments The authors acknowledge the financial support provided by both the Faculty of Sciences and the Department of Chemistry at Université du Québec à Montréal. Graduate student L. Barhoumi is thankful to the Faculty of Science of University of Bizerte and to the Ministère de L'Enseignement Supérieur et de la Recherche Scientifique for providing a fellowship.

References

Ait Ali N, Dewez D, Didur O, Popovic R (2006) Inhibition of photosystem II photochemistry by Cr is caused by the alteration of D1 protein and oxygen evolving complex. Photosynth Res 89:81–87

Appenroth K-J, Stöckel J, Srivastava A, Strasser RJ (2001) Multiple effects of chromate on the photosynthetic apparatus of *Spirodela polyrhiza* as probed by OJIP chlorophyll *a* fluorescence measurements. Environ Pollut 115:49–64

Aruoja V, Dubourguier H-C, Kasemets K, Kahru A (2009) Toxicity of nanoparticles of CuO, ZnO and TiO_2 to microalgae *Pseudokirchneriella subcapitata*. Sci Total Environ 407:1461–1468

Babu TS, Akhtar TA, Lampi MA, Tripuranthakam S, Dixon DG, Greenberg BM (2003) Similar stress responses are elicited by copper and ultraviolet radiation in the aquatic plant *Lemna gibba*? Implication of reactive oxygen species as common signals. Plant Cell Physiol 44:1320–1329

Baker NR (2008) Chlorophyll fluorescence: a probe of photosynthesis *in vivo*. Ann Rev Plant Biol 59:89–113

Basti H, Tahar LB, Smiri LS, Herbst F, Vaulay MJ, Chau F, Ammar S, Benderbous S (2010) Catechol derivatives-coated Fe_3O_4 and gamma-Fe_2O_3 nanoparticles as potential MRI contrast agents. J Colloid Interface Sci 341:248–254

Ben Tahar L, Basti H, Herbst F, Smiri LS, Quisefit JP, Yaacoub N, Grenèche JM, Ammar S (2012) $Co_{1-x}Zn_xFe_2O_4$ ($0 \leq x \leq 1$) nanocrystalline solid solution prepared by the polyol method: characterization and magnetic properties. Mater Res Bull 47: 2590–2598

Bhatt I, Tripathi BN (2011) Interaction of engineered nanoparticles with various components of the environment and possible strategies for their risk assessment. Chemosphere 82:308–317

Chen X, Zhu X, Li R, Yao H, Lu Z, Yang X (2012) Photosynthetic toxicity and oxidative damage induced by nano-Fe_3O_4 on *Chlorella vulgaris* in aquatic environment. Op J Ecol 2:21–28

Dewez D, Geoffroy L, Vernet G, Popovic R (2005) Mechanism of fungicides action may determine biomarkers sensitivity indicating inhibitory effects: photosynthetic and enzymatic parameters used to determine fludioxonil and copper toxicity on alga *Scenedesmus obliquus*. Aquat Toxicol 74:150–159

Dewez D, Ali NA, Perreault F, Popovic R (2007) Rapid chlorophyll *a* fluorescence transient of *Lemna gibbers* leaf as an indication of light and hydroxylamine effect on photosystem II activity. Photochem Photobiol Sci 6:532–538

Domingos RF, Tufenkji N, Wilkinson KJ (2009) Aggregation of titanium dioxide nanoparticles: role of a fulvic acid. Environ Sci Technol 43:1282–1286

Flinders C (2006) The potential for bioaccumulation, bioconcentration, and biomagnification of selected metals in an aquatic food chain: a literature review. NCASI Tech Bull 927:1–48

Frankart C, Eullaffroy P, Vernet G (2002) Photosynthetic responses of *Lemna minor* exposed to xenobiotics, copper, and their combinations. Ecotoxicol Environ Saf 53:439–445

Franklin NM, Rogers NJ, Apte SC, Batley GE, Gadd GE, Casey PS (2007) Comparative toxicity of nanoparticulate ZnO, bulk ZnO, and $ZnCl_2$ to a freshwater microalga (*Pseudokirchneriella subcapitata*): the importance of particle solubility. Environ Sci Technol 41:8484–8490

Gerst U, Schönknecht G, Heber U (1994) ATP and NADPH as the driving force of carbon reduction in leaves in relation to thylakoid energization by light. Planta 193:421–429

Griffitt RJ, Luo J, Gao J, Bonzongo J-C, Barber DS (2008) Effects of particle composition and species on toxicity of metallic nanomaterials in aquatic organisms. Environ Toxicol Chem 27:1972–1978

Hoffmann WA, Poorter H (2002) Avoiding bias in calculations of relative growth rate. Ann Bot 90:37–42

Hu X, Cook S, Wang P, Hwang HM (2009) *In vitro* evaluation of cytotoxicity of engineered metal oxide nanoparticles. Sci Total Environ 407:3070–3072

Jiang J, Oberdörster G, Biswas P (2009) Characterization of size, surface charge, and agglomeration state of nanoparticles dispersions for toxicological studies. J Nanopart Res 11:77–89

Klaine SJ, Alvarez PJJ, Batley GE, Fernandes TF, Handy RD, Lyon DY, Mahendra S, McLaughlin MJ, Lead JR (2008) Nanomaterials in the environment: behavior, fate, bioavailability, and effects. Environ Toxicol Chem 27:1825–1851

Küpper H, Šetlík I, Spiller M, Küpper FC, Prášil O (2002) Heavy metal-induced inhibition of photosynthesis: targets of in vivo heavy metal chlorophyll formation. J Phycol 38:429–441

Le Bail A (2004) Monte carlo indexing with mcmaille. Pow Diff 19:249–254

Lewis MA (1995) Use of freshwater plants for phytotoxicity testing: a review. Environ Pollut 87:319–336

Mayer P, Kuhel R, Nyholm N (1997) A simple in vitro fluorescence method for biomass measurements in algal growth inhibition tests. Water Res 31:2525–2531

Mushtaq YK (2011) Effect of nanoscale Fe_3O_4, TiO_2 and carbon particles on cucumber seed germination. J Environ Sci Health 46:1732–1735

OECD (2006) Guidelines for the testing of chemicals. *Lemna* sp. growth inhibition test. OECD, Paris

Peralta-Videa JR, Zhao L, Lopez-Moreno ML, de la Rosa G, Hong J, Gardea-Torresdey JL (2011) Nanomaterials and the environment: a review for the biennium 2008–2010. J Hazard Mater 186:1–15

Popovic R, Dewez D, Juneau P (2003) Application of chlorophyll *a* fluorescence parameters in ecotoxicological studies of pollutants: Heavy metals, herbicides and air pollutants. In: Toivonen P, DeEll J (eds) Practical applications of chlorophyll fluorescence in plant biology. Kluwer Academic, Dordrecht, pp 152–179

Ralph PJ, Smith RA, MacInnis-Ng CMO, Seery CR (2007) Use of fluorescence-based ecotoxicological bioassays in monitoring toxicants and pollution in aquatic systems: review. Toxicol Environ Chem 89:589–607

Scown TM, van Aerle R, Tyler CR (2010) Review: do engineered nanoparticles pose a significant threat to the aquatic environment? Crit Rev Toxicol 40:653–670

Seaton GGR, Walker DA (1990) Chlorophyll fluorescence as a measure of photosynthetic carbon assimilation. Proc R Soc Lond B Biol Sci 242:29–35

Singh N, Jenkins GJS, Asadi R, Doak SH (2010) Potential toxicity of superparamagnetic iron oxide nanoparticles (SPION). Nano Rev 1:5358

Strasser BJ, Strasser RJ (1995) Measuring fast fluorescence transients to address environmental questions: the JIP-test. In: Mathis P (ed) Photosynthesis: from light to biosphere, vol 5. Kluwer Academic, Dordrecht, pp 977–980

Strasser RJ, Srivastava A, Tsimilli-Michael M (2004) Chlorophyll fluorescence: A signature of photosynthesis, advances in photosynthesis and respiration. In: Papageorgiou G, Govindjee (eds) Analysis of the chlorophyll a fluorescence transient. Kluwer Academic, Dordrecht

Vaidyanathan S, Sendhilnathan R, Arulmurugan J (2007) Structural and magnetic properties of $Co_{1-X}Zn_XFe_2O_4$ nanoparticles by co-precipitation method. J Magn Magn Mater 313:293–299

Wellburn AR (1994) The spectral determination of chlorophyll *a* and *b*, as well as total carotenoids, using various solvents with spectrophotometers of different resolution. J Plant Physiol 144:307–313

Zhu H, Han J, Xiao JQ, Jin Y (2008) Uptake, translocation, and accumulation of manufactured iron oxide nanoparticles by pumpkin plants. J Environ Monit 10:713–717